Integration of Inertial Navigation into Real-Time GIPSY-x (RTGx)

Jason N. Gross, Ryan M. Watson, Victor Sivaneri *West Virginia University*
Yoaz E. Bar-Sever, William I. Bertiger, Bruce Haines *Jet Propulsion Laboratory*

ABSTRACT

This paper details the integration of an Inertial Navigation System (INS) processing capability within JPL's RTGx geodetic data analysis and navigation software, and provides a performance analysis with experimental flight data in order to validate the implementation. The RTGx software, when used in conjunction with JPL's Global Differential GPS System (GDGPS), can be configured for real-t ime kinematic Precise Point Positioning (K-PPP) for centimeter-level positioning accuracy. Since 2006, RTGx's predecessor, RTG, has provided operational real-time K-PPP for NASA's Uninhabited Aerial Vehicle Synthetic Aperture Radar (UAVSAR) repeat pass interferometry mission on campaigns all over the world. While RTG's GPS-only data processing is meeting mission requirements during nominal science operations, its performance naturally degrades during certain flight scenarios, such as abrupt changes in the aircraft attitude or high banking turns, which induce signal loss-of-lock, carrier-phase breaks and/or cycle slips. During these periods, the well-known downsides of K-PPP, including the position solution's sensitivity to phase breaks and slow convergence after loss-of-lock become apparent, and may impact the instruments critical data take periods. Therefore, tightly-coupled INS has been integrated into RTGx to offer additional robustness. This paper discusses the adopted INS formulation and uses the flight data made available to the community by the National Geodetic Survey's Kinematic Challenge (Damiani et al., 2013) to offer an experimental performance evaluation. The integration of INS in RTGx is shown to provide solution improvements both in terms of accuracy and precision with respect to a post- processed ambiguity-fixed reference solution. Furthermore, the integration of INS into the RTGx software will enable RTGx to support new application domains.

1 INTRODUCTION

1.1 Background and Motivation

It is well known that GPS PPP-based real-time positioning techniques are sensitive to dropped satellite observations and carrier phase breaks (Bisnath and Gao, 2009). To address this, recent studies have shown that multi-constellation GNSS can improve K-PPP position solution convergence rate (Cai et al., 2015) and offer better positioning performance when working with relatively short observation durations (Yigit et al., 2014). Likewise, the incorporation of Inertial Navigation Systems (INS) within K-PPP has also been shown to offer faster solution convergence, better recovery from cycle slips, and improved robustness to signal blockage providing performance that is comparable conventional local-area Real-Time Kinematic (RTK)/INS solutions (Zhang and Gao, 2008).

RTGx (Bar-Sever et al., 2015) is JPL's new GNSS processing software that can be configured for real-time or post-processed constellation orbit and clock determination, Low-Earth Orbiter (LEO) Precise Orbit Determination, or Precise Point Positioning (PPP). RTGx underlies the navigation software for the Air Force's next generation GPS operational control segment (OCX) (Bertiger et al., 2012). In conjunction with JPL's GDGPS System, where RTGx generates the real-time GNSS orbit and clocks products, and is also the point-positioning engine, RTGx routinely and operationally produces sub-decimeter real-time kinematic positioning for a large number of GNSS tracking sites, globally [www.gdgps.net].

Different from its predecessor, RTGx now supports a multi-constellation GNSS processing capability, thus, an additional natural evolution of the RTGx software is to support an INS capability for kinematic applications that have demanding requirements. While tight GNSS/INS integration is by no means a new concept, integration of INS within RTGx inherits features that are already unique to JPL's RTGx processing strategy, such as single-receiver integer ambiguity resolution (Bertiger et al., 2010) as well as flexible and easily extendable parameter and model configuration. Incorporation of INS in RTGx will further enable research in more advanced INS/GNSS models, such as solving for deviations of the local gravity error, processing platforms with multiple antennas, leveraging atomic clocks, ingesting pressure sensor data for troposphere modeling, solving for unknown IMU lever arms, and processing kinematic platforms as part of a network solution, all of which which can contribute to increased accuracy required by various science applications.

This paper presents the details of an baseline implementation of INS within RTGx and offers a validation of its performance by processing flight data from the National Geodetic Survey's (NGS) Kinematic Challenge (NGS, 2011). The use of the NGS Kinematic Challenge data enables performance comparisons against a post-processed carrier-phase ambiguity fixed (Bertiger et al., 2010) reference solution that was processed by JPL researchers using GIPSY-OASIS II and has been vetted for accuracy through a comparison with several other post-processed solutions contributed by the research community who used various GPS software packages and differential processing techniques as part of the Kinematic Challenge (Damiani et al., 2013). For this experimental data analysis, forward-filter only K-PPP performance with and without the inclusion of INS is assessed against the reference solution. Furthermore, RTGx/INS filter-only platform attitude estimates are compared with the smoothed best estimates of the commercially available GPS/INS attitude solution flown in NGS GRAV-D aircraft.

The immediate need for this work was motivated by the NASA JPL's Uninhabited Aerial Vehicle Synthetic Aperture Radar (UAVSAR) project. UAVSAR is an airborne L-band Synthetic Aperture Radar (SAR) platform that has relied upon RTG and GDGPS to provide real-time position feedback for guiding a precision platform auto-pilot since the project's inception in 2006 (Rosen et al., 2006). The UAVSAR application is particularly well-suited for using K-PPP because it requires real-time positioning with global-availability in order to support rapid response to natural hazard events (e.g. earth quakes, volcanic activity) over remote locations, thus precluding the use of RTK with a reference station. The primary need of real-time positioning on UAVSAR is to guide a precision autopilot in order to ensure that the platform flies the same trajectory between subsequent visits to a particular campaign site. Operationally, throughout the UAVSAR project, it has been the case that immediately before the autopilot is engaged for a radar data-take, an abrupt aircraft bank occurs, which induces dropped satellites and/or carrier phase breaks. This, in turn, degrades the positioning performance, and because of this, the real-time K-PPP solution is often in the process of re-converging to its achievable centimeter-level performance during the short period of time in which is most critical for real-time observations. By including INS in RTGx, it is expected to increase the robustness of the real-time positioning solution.

The rest of this paper is organized as follows. The next section describes the integration architecture and INS formulation implemented in RTGx. Then, the contents of the NGS Kinematic Challenge data are reviewed. Finally, both sets of flight data are used to validate the performance of the INS implementation in RTGx and the next steps of this work are summarized.

2 ALGORITHM FORMULATION

This section describes the PPP/INS integration architecture selected for RTGx, as well as the details of the selected INS formulation. The algorithmic details of the PPP models and observation equations are not reviewed in this paper, as these were not modified in RTGx as part of this work.

2.1 Integration Architecture

The integration architecture adopted for RTGx is an INS error-state formulation with closed-loop feedback correcting the integrated INS solution at each time-step (Groves, 2013) as shown in Figure 1.

As shown in Figure 1, the INS estimated navigation states are used to predict GNSS observables within the Kalman Filter (i.e. in the case of RTGx a Square Root Information Filter (Bierman, 2006) formulation is used). Using the difference between the two data sources, error-states of the INS solution along with some standard PPP states (i.e. receiver clock model states, phase biases and zenith tropospheric delay) are estimated. The overall estimated state vector is shown in Eq. 1, and is comprised of:

- $\delta\Psi$ - INS attitude error;
- δv - INS velocity error;
- δr - INS position error;
- b_a - three Inertial Measurement Unit (IMU) tri-axial accelerometer sensor biases;
- b_g - three IMU tri-axial gyroscope sensor biases;
- δt_u - the estimated receiver clock bias;
- $\dot{\delta t_u}$ - the estimated receiver clock drift;
- T_w - the estimated residual tropospheric delay along the zenith direction;
- $N_{1\ldots j}$ - estimated phase bias for each satellite in view.

$$\mathbf{x} = \begin{pmatrix} \delta\Psi \\ \delta v \\ \delta r \\ b_a \\ b_g \\ \delta t_u \\ \dot{\delta t_u} \\ T_w \\ N_1 \\ \vdots \\ N_j \end{pmatrix} \tag{1}$$

It can also be seen in Figure 1 that the estimated IMU sensor biases are fed back to correct the raw IMU measurements. Feedback of both the INS error-states and the IMU sensor biases is done every time that a GNSS measurement

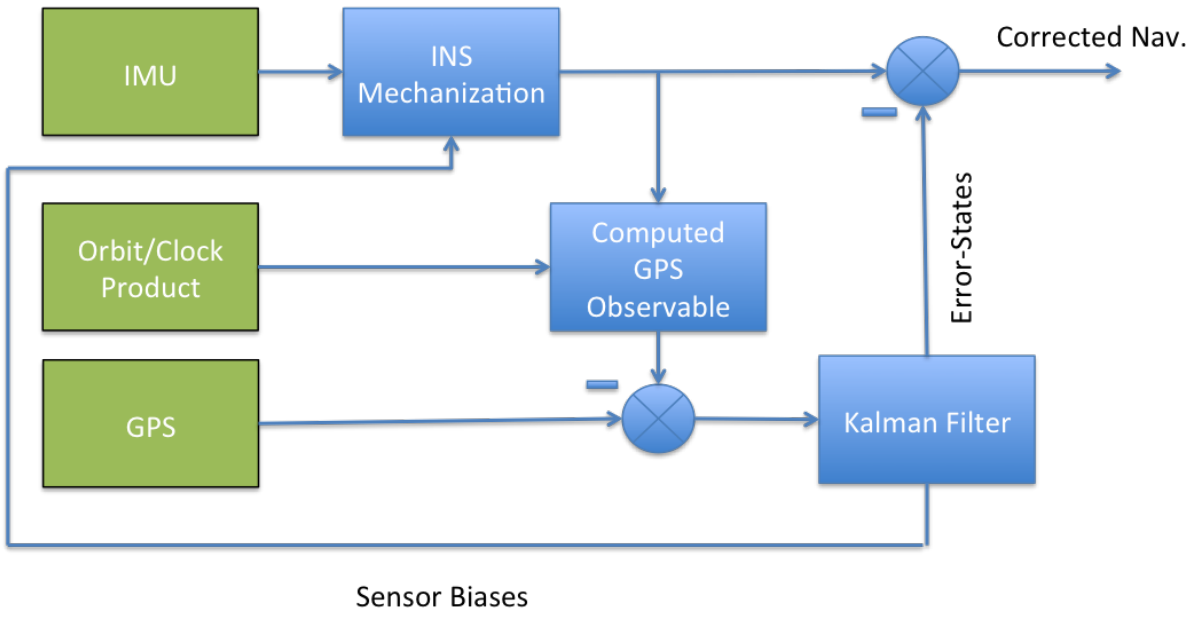

Figure 1. RTGx INS integration architecture. Error-states to the INS and IMU sensor biases are estimated and fed-back in a closed-loop manner to correct the navigation states.

update is performed. For the position and velocity, the estimated error-states δr and δv are used to correct the INS position and velocity by simply adding the solved for delta to the INS state. The attitude estimated error-state is applied to the INS attitude using a small-angle approximation as shown in Eq. 2

$$C_i^b = (I - \delta\Psi) * \hat{C}_i^b \tag{2}$$

where $\hat{C}_i^b$ is the DCM populated with the INS estimated quaternion, which is described in the next section.

2.2 Inertial Navigation System Mechanization

Since Newton's equations of motion are simplest in an inertial reference frame and RTGx already deals with Earth orbiting satellites, the natural reference frame for it's models is an Earth Centered Inertial frame. Thus we adopt, an Earth Centered Inertial (ECI) frame to mechanize the INS model. The inertial navigation mechanization equations are derived in many technical references (Groves, 2013; Jekeli, 2001), and summarized here.

2.2.1 Attitude Update

To perform the attitude update, a 3rd order fixed-step Runge-Kutta integration method was chosen for the integration of the quaternion that represents the aircraft's body attitude in an ECI frame. The specific integrator used is detailed in the INS for Geodetic Applications text written by Jekeli (Jekeli, 2001), which is shown to limit the algorithmic integration errors to the fourth order. The quaternion is integrated using Eq. 3: where I is an identity matrix, β is composed of the delta theta IMU measurements (i.e. incremental body-axis angular rate integrations over the IMU sample rate interval) within the aircraft body-axes in Eq. 4, and the subscript t signifies the IMU time step (e.g. $t-2$ is using data from two discrete sample intervals in the past).

The platform's body-to-ECI direction cosine matrix (DCM) C_b^i is then related to the updated quaternion using standard attitude representation transformations found in many aerospace texts (Stevens and Lewis, 2003; Markley and Crassidis, 2014). Furthermore, upon quaternion integration, it is possible that integration error and/or the noisy IMU measurements will lead to quaternion that does not represent an orthonormal transformation. In order to prevent this, the quaternion is periodically normalized to unity.

2.2.2 Velocity Update

Once the IMU delta angles have been integrated to update the INS attitude estimates, the IMU accelerometer's specific force measurements must be transformed from the body-axis to the ECI frame before integration. Like IMU angular rates, high-grade IMUs typically provide acceleration measurements in the form of incremental changes to the body-axis velocity Δv_b, which are internally integrated within the IMU over the sample interval. The transformation was conducted by simply multiplying IMU measurements by the body-to-ECI DCM, C_b^i, as shown in Eq. 5.

$$\Delta v^i = C_b^i \Delta v^b \tag{5}$$

With the transformed specific force, INS velocity is determined through a simple integration as shown in Eq. 6.

$$\hat{q}_t = [I + \frac{1}{12}(\hat{B}_t + 4\hat{B}_{t-1} + \hat{B}_{t-2}) + \frac{1}{12}(I + \frac{1}{4}\hat{\beta}_t)\hat{\beta}_{t-1}\hat{\beta}_{t-2} + \frac{1}{12}\hat{\beta}_t(\hat{\beta}_{t-1} - \frac{1}{2}\hat{\beta}_{t-2})]\hat{q}_{t-2} \tag{3}$$

$$\hat{\beta}_{t+1-n} = \begin{bmatrix} 0 & (3(\delta\theta_1)_{t+1-n} - (\delta\theta_1)_{t-n}) & (3(\delta\theta_2)_{t+1-n} - (\delta\theta_2)_{t-n}) & (3(\delta\theta_3)_{t+1-n} - (\delta\theta_3)_{t-n}) \\ (-3(\delta\theta_1)_{t+1-n} + (\delta\theta_1)_{t-n}) & 0 & (3(\delta\theta_3)_{t+1-n} - (\delta\theta_3)_{t-n}) & (-3(\delta\theta_2)_{t+1-n} + (\delta\theta_2)_{t-n}) \\ (-3(\delta\theta_2)_{t+1-n} + (\delta\theta_2)_{t-n}) & (-3(\delta\theta_3)_{t+1-n} + (\delta\theta_3)_{t-n}) & 0 & (3(\delta\theta_1)_{t+1-n} - (\delta\theta_1)_{t-n}) \\ (-3(\delta\theta_3)_{t+1-n} + (\delta\theta_3)_{t-n}) & (3(\delta\theta_2)_{t+1-n} - (\delta\theta_2)_{t-n}) & (-3(\delta\theta_1)_{t+1-n} + (\delta\theta_1)_{t-n}) & 0 \end{bmatrix} \tag{4}$$

In Eq. 6, the updated INS velocity estimate is the summation of the previous velocity value $(k-1|k-1)$ and the IMU measured change in velocity, Δv^i. In addition, the acceleration due to gravity, which cannot be explicitly measured by the IMU, must be modeled and represented in ECI components, denoted by γ^i in Eq. 6, and integrated over the INS integration internal τ.

$$v^i_{k|k-1} = v^i_{k-1|k-1} + \Delta v^i + \gamma^i \tau \tag{6}$$

For modeling gravity, the model specified in the 2010 IERS conventions was adopted (Petit and Luzum, 2010).

2.2.3 Position Update

Finally, the position in an ECI frame is updated by simply integrating from the previous position estimate with the average velocity over the INS integration interval. For this integration, trapezoidal integration is used by averaging the previous velocity estimate and the updated velocity estimate.

$$r^i_{k|k-1} = r^i_{k-1|k-1} + (v^i_{k|k-1} + v^i_{k-1|k-1})\frac{\tau}{2} \tag{7}$$

2.3 Error-State Extended-Kalman Filter

To calculate INS error-state system matrix, F, the derivative of each error-state model equation with respect to each solved for parameter must be taken. In this section, the derivative of the attitude, velocity, and position equations are described as derived by Groves (2013). After defining the time derivatives of the error state equations, the total system matrix and the state transition matrix (STM), Φ^i, is defined.

The time derivative of the attitude error can be seen in Eq. 8: where $\hat{C}^i_b$ is the estimated body-to-ECI DCM, and b_g is the estimated bias on the IMU body-axis gyroscopes.

$$\delta\dot{\Psi}^i = \hat{C}^i_b b_g \tag{8}$$

The velocity error-state derivative is dependent on the accelerometer biases, gyroscope biases, as well as the gravity model that is employed. Eq. 9 shows this time derivative of the velocity error equation, $\delta\dot{v}^i$. In this implementation, the gravity model partials used the simplified model offered by Groves (2013).

In Eq. 9, $\hat{f}^i$ is the IMU accelerometer measured specific force in the inertial frame (i.e. $\delta v/\tau$), $\delta\Psi^i$ is the current estimated attitude error, g is the estimated gravity vector for the platform's position, r^e_{es} is the geocentric radius at the platform position, $\hat{r^i}$ is the INS estimated position vector, δr^i_{ib} is the estimated position error, and the vector b_a represents the estimated accelerometer sensor biases in units of m/s^2 (i.e. note that accelerometer biases are still modeled in units of acceleration although delta-velocity measurements are being processed from the IMU).

$$\delta\dot{V}^i = -(\hat{C}^i_b\hat{f}^i)\delta\Psi^i + \frac{2g}{r^e_{es}}\frac{\hat{r^i_{ib}}}{|\hat{r^i_{ib}}^2|}\hat{r^i}^T\delta r^i + \hat{C}^i_b b_a \tag{9}$$

With INS mechanized in an inertial frame, the time-derivative of position is simply velocity, such that the time-derivative of the position error is the velocity error.

$$\delta\dot{r}^i = \delta V^i \tag{10}$$

Using the time derivative of each error-state equation, the system matrix is defined in Eq. 11, as also given in (Groves, 2013).

$$F^i = \begin{bmatrix} 0_3 & 0_3 & 0_3 & 0_3 & \hat{C}^i_b \\ -(\hat{C}^i_b\hat{f}^i) & 0_3 & \frac{2g}{r^e_{es}}\frac{\hat{r^i}}{|\hat{r^i}^2|}\hat{r^i}^T & \hat{C}^i_b & 0_3 \\ 0_3 & I_3 & 0_3 & 0_3 & 0_3 \\ 0_3 & 0_3 & 0_3 & 0_3 & 0_3 \\ 0_3 & 0_3 & 0_3 & 0_3 & 0_3 \end{bmatrix} \tag{11}$$

The discretized STM is then calculated using a power-series expansion of system matrix as shown in Eq. 12, where a third order expansion leads to Eq. 13. Where the notation is such that F^i_{21} and F^i_{23} correspond to the value of the system matrix at the specified row and column.

$$\Phi = e^{F^i\tau} \tag{12}$$

$$\Phi^i = \begin{bmatrix} I_3 & 0_3 & 0_3 & 0_3 & \hat{C}^i_b\tau \\ (F^i_{21}\tau + \frac{1}{6}F^i_{23}F^i_{21}\tau^2) & (I_3 + \frac{1}{2}F^i_{23}\tau^2) & (F^i_{23}\tau + \frac{1}{6}{F^i_{23}}^2\tau^3) & (\hat{C}^i_b\tau + \frac{1}{6}F^i_{23}\hat{C}^i_b\tau^3) & (\frac{1}{2}F^i_{21}\hat{C}^i_b\tau^2) \\ (\frac{1}{2}F^i_{21}\tau^2) & (I_3*\tau + \frac{1}{6}F^i_{23}\tau^3) & (I_3*+\frac{1}{2}F^i_{23}\tau^2) & (\frac{1}{2}\hat{C}^i_b\tau^2) & (\frac{1}{6}F^i_{21}\hat{C}^i_b\tau^3) \\ 0_3 & 0_3 & 0_3 & I_3 & 0_3 \\ 0_3 & 0_3 & 0_3 & 0_3 & I_3 \end{bmatrix} \tag{13}$$

2.4 Processing Rate

Within this selected INS formulation, because a Runge-Kutta method relies on the availability of mid-points is adopted for attitude integration, the INS navigation states are propagated at a rate half of the available IMU data rate. That is, in the case of the data presented in this paper both simulated and the Kinematic Challenge flight data, 200 Hz IMU data is used to predict attitude, position and velocity at a rate of 100 Hz.

2.5 IMU to GNSS Lever Arm

The above INS mechanization provides estimates of the position and velocity located at the center of the IMU. In order to combine with GNSS measurements, the INS solution must be transposed to the GNSS antenna location. This can be done using the estimated platform attitude $\hat{C}_b^i$ and knowledge of the lever arm from the IMU to the GNSS antenna, L_b, represented in the platforms North, East, Down (NED) body-axis.

$$r_{k|k-1}^{i,GNSSAnt.} = r_{k|k-1}^{i,IMU} + \hat{C}_b^i L_b \tag{14}$$

Likewise the velocity can be transposed further taking into consideration the rotation of the body-frame.

$$v_{k|k-1}^{i,GNSSAnt.} = v_{k|k-1}^{i,IMU} + \hat{C}_b^i \Omega_{ib}^b L_b \tag{15}$$

where Ω_{ib}^b is the skew-symmetric matrix of the IMU measured angular rate that has been calibrated by the estimated gyroscope biases. The operation is performed upon each GNSS measurement update, and reversed after closed-loop feedback correction has been applied, in order to resume INS integration about the location of the IMU. For the NGS Kinematic Challenge data, the precisely measured IMU to GPS antenna lever arm was provided, however, the lever arm as been included as a potentially solved for parameter in the RTGx implementation.

2.6 GNSS/IMU Measurement Time-Alignment

Most commercially available high-accuracy GNSS/IMU systems provide IMU measurements precisely stamped to the GPS time- scale, however, the IMU measurements are typically not scheduled to be precisely aligned with the GPS measurement epochs. To ensure time-alignment in the RTGx implementation, the IMU data was used to predict the navigation state to an epoch just past the GNSS observation epoch. This prediction was then used to linearly interpolate the navigation states back to the time of the GNSS measurements. Likewise, upon each GNSS update, an error-state transformation matrix, that provides the mapping of the INS error-states between the INS time-step (that is just past the GNSS measurement epoch), and the exact GNSS measurement epoch was derived. Prior to the GNSS update, the inverse of this transformation was used to downdate the predicted INS error-states to the GNSS measurement epochs. After the update was completed, this transformation was used to keep the INS error states consistent with the INS time-tags.

3 ALGORITHM PERFORMANCE EVALUATION

For initial validation, a comprehensive performance characterization was conducted using simulated flight data. This simulation study is detailed by Watson et al. 2016. Here we discuss evaluation using the NGS Kinematic Challenge Data.

3.1 Flight Data

The NGS Kinematic Challenge (NGS, 2011; Damiani et al., 2013) data sets includes two seperate data sets of

- 1 Hz dual-frequency GPS pseudorange and carrier-phase observables
- 200 Hz GPS time-stamped IMU measurements
- surveyed lever arm between the platform's instrument and GPS Antenna, and between the instrument and the IMU
- the commercial GNSS/INS systems smoothed attitude estimates

In addition, a few GPS reference station data sets are provided for deriving network-based or RTK solutions, however the base-station data was not used in the analysis presented in this paper. The two flight profiles are very similar. Figure 2 shows the altitude profile of the first data set.

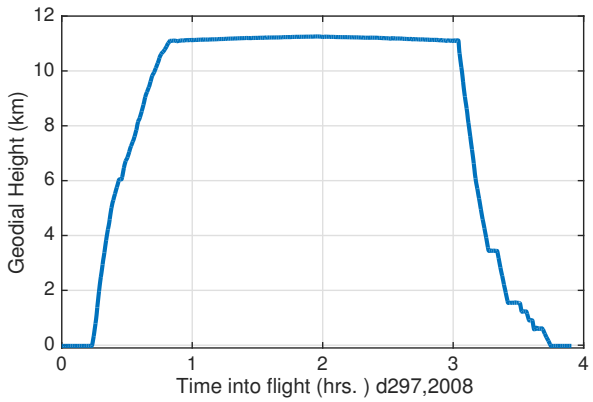

Figure 2. Altitude profile of the d297,y2008 Kinematic Challenge data-set. The aircraft rapidly ascends from sea-level to an altitude of 11 km and then back to sea-level, which is particularly challenging for handling the estimation of the tropospheric delays of the GPS observables.

Furthermore, the flight profiles consist of long duration steady-level legs at almost precisely due-North/South and due-East/West. These directional legs are particularly

useful for validating common GNSS/INS issues, such as properly handling time-alignment and the sensor lever arms. Figure 3 shows the Lat./Lon. profile of the flights.

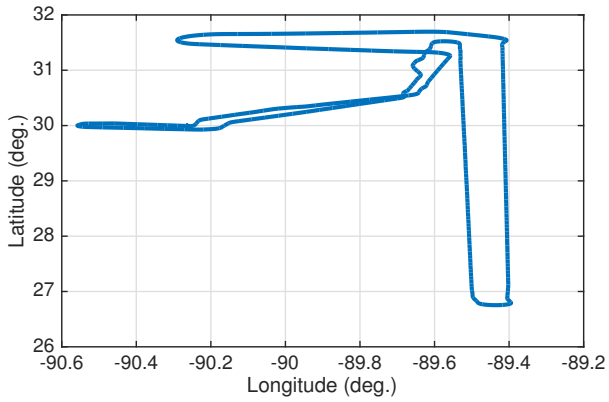

Figure 3. Lat/Lon profile of d297,y2008 Kinematic Challenge data-set. The aircraft traverses in straight legs in North/South and East/West which is beneficial for uncovering systematic errors such as, incorrect lever-arm and time mis-alignment.

3.2 Reference Solutions

In order to provide a reference position solution for validating the filter-only PPP/INS solution, JPL's post-processed submissions's to the NGS Kinematic Challenge were used. These solutions were processed with JPL's GIPSY-OASIS II software, and featured carrier-phase integer bias-fixing using JPL's Wide-Lane Phase Bias products (Bertiger et al., 2010). Furthermore, GNSS data-outliers were deleted from the final solution using an iterative windowing approach.

The reference platform attitude solution used in this analysis is the smoothed best estimate solution provided by the Applanix PosAV software and included in the Kinematic Challenge data sets.

3.3 Processing Strategy

In this analysis, two solutions are compared to the reference position solutions, namely K-PPP with INS and K-PPP without INS. The analysis considers the performance of the forward-filter only solutions, as this is most applicable to the real-time needs of the target application for this work, UAVSAR. This section described the distills of processing strategies adopted.

For both filter-only K-PPP strategies, prior to processing with RTGx, the RINEX data were pre-processed by GIPSY's GPS data editor in order to remove gross-outliers and flag carrier-phase breaks (Blewitt, 1990). In addition, for all runs with and without INS, a simple troposphere estimation strategy that solves for a residual wet zenith delay as a random walk parameter was adopted. This value was empirically tuned to provide smooth estimation performance when at altitude and selected to be 5e-5 $\frac{m}{\sqrt{s}}$. Furthermore, for both cases, with and without INS, the GPS receiver clock was modeled as a random walk process with 100 $\frac{m}{\sqrt{s}}$. Finally, all solutions used JPL's final orbit/clock submissions to the International GNSS Service (Desai et al., 2011).

For designing the INS stochastic models, typically the sensor specs of the individual IMU sensors (e.g. Angular Random Walk, Velocity Random Walk, bias-instabilities) would be used to drive these models (Gross et al., 2011). However, for the Applanix PosAV GPS/IMU system used in the Kinematic Challenge data set, these IMU sensor parameters were unknown. Therefore, these parameters were initially selected assuming an intermediate grade IMU and then empirically tuned.

Finally, in order to provide better comparison and aid in the convergence of the GPS-only K-PPP strategy, a dual-frequency pseudorange-only solution was ingested as the *a priori* nominal position solution with the filter-only runs. The carrier-phase based K-PPP positions were then solved as for assuming 10 meters of uncertainty in the nominal solution at each data epoch.

4 RESULTS AND DISCUSSION

The key statistics with respect to positioning accuracy and attitude estimation are summarized in this section. For positioning, the metrics selected include:

- Root Mean Square (RMS)
- Standard Deviation (σ)
- Average Bias ($b_{E,N,U}$)
- Max absolute error ($Max(|b_{E,N,U}|)$)

For this analysis, all errors are reported with respect to the reference solutions and are decomposed into their East, North and Vertical components. Furthermore, these metrics are reported after initial solution convergence until the end of the data sets. The convergence period was excluded because the most crucial period during airborne science campaigns is after ascending to the final altitude. In this analysis, this was done by simply by evaluating errors over only the last 2/3 of each flight.

For attitude error analysis, RMS stats of the platforms roll, ϕ, pitch, θ, and heading ψ are reported with respected to the Applanix posAV solution are reported.

Finally, a few internal metrics that proved useful through the integration/debugging of the INS integration in RTGx are summarized. These include postfit data residuals, and statistics of the average solution corrections (i.e. $\Delta =$ Nominal - Adjusted Solution) for the 3 position axes.

4.1 Positioning Performance with Respect to Reference Solution

Table 1 suggests that the K-PPP solution is significantly smoother and more accurate with respect to the post-processed

Table 1. Statistics of positioning performance for d297 Kinematic Challenge Data Set

Filter-Only	K-PPP/INS	K-PPP
East RMS (cm)	6.1	12.8
North RMS (cm)	4.1	7.6
Vertical RMS (cm)	26.7	51.9
East σ (cm)	3.4	8.1
North σ (cm)	2.5	3.4
Vertical σ (cm)	17.5	51.7
b_{East} **(cm)**	-5.0	-10.0
b_{North} **(cm)**	3.2	6.8
$b_{Vertical}$ **(cm)**	-20.2	-4.1
Max($\lvert b_{East} \rvert$**) (cm)**	17.1	24.2
Max($\lvert b_{North} \rvert$**) (cm)**	10.8	14.0
Max($\lvert b_{Vertical} \rvert$**) (cm)**	48.4	153.3

reference solution. Against all of the metrics, the solution with INS outperformans the non-INS case. However, one potentially misleading value is that the vertical mean bias with respect to the reference solution is significantly smaller for the non-INS case. Figure 4 suggests that this is due to the GPS-only solution to not being able to keep up with the increased tropospheric delay during the aircraft descent.

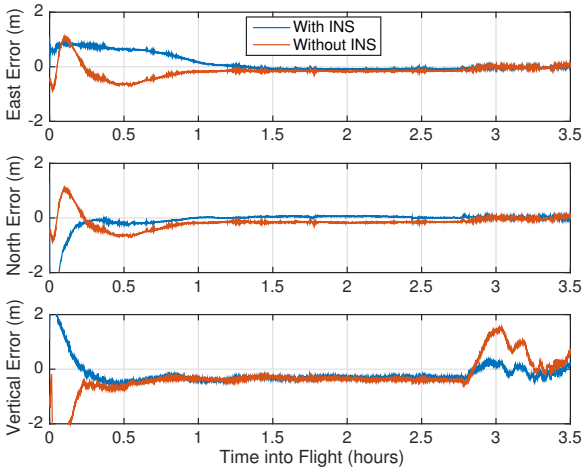

Figure 4. ENU components of position error for K-PPP with and without INS for the d297 flight. At ≈ 2.75 hours into the flight, the aircraft begins to descend. Both errors increase significantly, but the solution with INS is able to reduce the error growth as the tropospheric delay is rapidly increasing.

While it is certainly true that a more sophisticated tropospheric modeling method could have been adopted, this serves to show a benefit of incorporating INS into the PPP solution. For example, increasing the process noise for the zenith delay could have avoided this occurring during descent phase, but this would have come at the expense of noisier vertical estimation when the aircraft was flying long durations at the 11 km altitude.

Table 2 presents the same metrics for d324, y2008 Kinematic Challenge data set.

Table 2. Statistics of positioning performance for d324 Kinematic Challenge Data Set

Filter-Only	K-PPP/INS	K-PPP
East RMS (cm)	7.5	7.0
North RMS (cm)	2.3	6.2
Vertical RMS (cm)	12.4	30.6
East σ (cm)	7.5	4.8
North σ (cm)	2.1	5.6
Vertical σ (cm)	12.1	26.7
b_{East} **(cm)**	-0.3	5.2
b_{North} **(cm)**	1.0	-2.6
$b_{Vertical}$ **(cm)**	2.6	15.0
Max($\lvert b_{East} \rvert$**) (cm)**	39.1	38.2
Max($\lvert b_{North} \rvert$**) (cm)**	59.7	59.7
Max($\lvert b_{Vertical} \rvert$**) (cm)**	82.4	149.7

Just as Table 1, Table 2, indicates that in general, incorporating INS increased positioning performance with respect to the reference solution. For d324, this is more prevalent in the North and Vertical components, and in fact, the East component is actually 0.5 cm worse in an RMS sense with respect to the reference solution. This can be attributed to a slightly slower, but much more stable, of the East component of the INS solution with respect to the solution without INS. This is illustrated in Figure 5.

4.2 Attitude Estimation with Respect to Reference Solution

This section is included as another means to experimentally validate the implementation on INS in RTGx, but obviously only the solutions that included INS will have attitude estimates. The RMS agreement with the smoothed Applanix PosAV attitude solutions provided in the Kinematic Challenge data sets are shown for d297 and d324 in Tables 3 and 4 respectively.

Table 3. Statistics of attitude estimation with respect to smoothed Applanix solution for d297,y2008

Filter-Only	K-PPP/INS
RMS Roll (deg.)	0.07
RMS Pitch (deg.)	0.15
RMS Yaw (deg.)	0.67

Tables 3 and 4 show very good agreement with respect to the attitude provided by the Applanix system. It should be noted that for flights that are primarily flying straight and level that it is well known that the IMU yaw-bias is most difficult to observe.

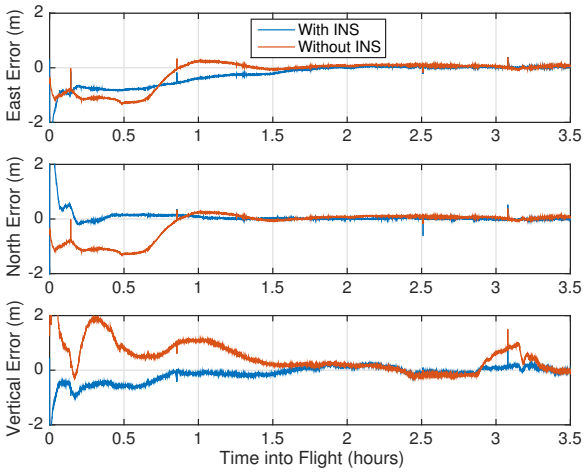

Figure 5. ENU components of position error for K-PPP with and without INS for the d324 flight. The solution with INS converges in a more stable manner that the non-INS solution, but has a slightly longer time constant. This leads to the 0.5 cm increase in RMS with evaluating errors over the last 2/3 of the flight.

Table 4. Statistics of attitude estimation with respect to smoothed Applanix solution for d324,y2008

Filter-Only	K-PPP/INS
RMS Roll (deg.)	0.06
RMS Pitch (deg.)	0.24
RMS Yaw (deg.)	1.01

4.3 Additional Metrics to Validate INS Implementation

Throughout the debugging of the integration of INS into RTGx, a few internal quality metrics were used to assess if the INS system was properly integrated. The first of these is simply evaluating statistics on the solved for position errors with respect to the INS provided nominal values. That is, how much did the GPS data have to correct about the INS nominal. For completeness, these are compared to the same metric for the GPS-only case, however, for the GPS-only K-PPP run the nominal was provided by a pseudorange-only solution. Table 5 shows an RMS summary of the solved for position deltas with respect to the INS solution and the pseudorange-only solution, respectively.

Table 5. Statistics ofΔ X,Y,Z for d297 flight. The INS is able to predict the corrected position within $\approx$ 10 cm.

Filter-Only	K-PPP/INS	K-PPP
RMS ΔX_{ECEF} (cm)	4.28	119.0
RMS ΔY_{ECEF} (cm)	9.6	193.15
RMS ΔZ_{ECEF} (cm)	8.38	139.9

In Table 5, not surprisingly, the pseudorange-only solution is accurate to only a few meters, leading to solved for position delta's at the same level. However, given the INS solution is able to provide a predicted solution much closer to the solved-for solution, leading to only centimeter level position adjustments.

Finally, spread of the pseudorange and carrier phase postfit residuals provides an additional mechanism to determine if there is a large systematic error in the processing strategy. Table 6 compares the standard deviations of the postfit GPS data residuals from the filter runs.

Table 6. Postfit residuals for d297 flight.

Filter-Only	K-PPP/INS	K-PPP
Phase (cm)	1.51	4.26
Range (m)	1.84	1.80

The significantly large spread of the phase residuals for the non-INS case is attributed to the periods of flight in which the tropospheric error is rapidly changing (accent and descent). This is illustrated in Figure 6

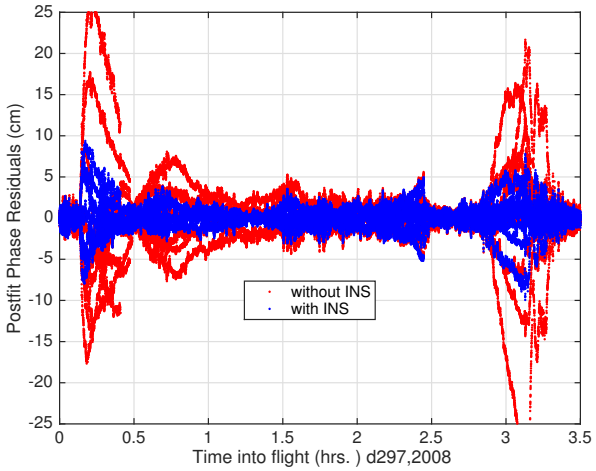

Figure 6. GPS Carrier-Phase residuals with and without including INS for d297, y2008 Kinematic Challenge flight. The non-INS phase residuals show large systematic errors during the aircraft take-off and ascent due to the rapidly changing troposphere delay.

Again, a more sophisticated troposphere delay modeling approach and inclusion of a pressure altimeter could be adopted to mitigate this for the GPS-only case, but Figure 6 serves to illustrate an advantage of including INS. These metrics for the d324,y2008 are nearly identical as the d297 data and are therefore omitted for brevity.

5 CONCLUSIONS AND FUTURE WORK

An INS processing capability has been integrated in JPL's RTGx GNSS processing software and its implementation

has been validated using real flight data. This paper described the integration architecture and specific INS mechanization used. In general, as expected, including INS leads to smoother and slightly more accurate position estimation performance. This work has been done to specifically address the needs of the NASA UAVSAR project, but will open RTGx to new applications including the processing of kinematic ocean buoys and Earth-quake monitoring with K-PPP/INS. Furthermore, it provides a basis to explore real-time signal receiver integer ambiguity resolution approaches.

ACKNOWLEDGEMENTS

This work was supported through a subcontract with the California Institute of Technology Jet Propulsion Laboratory which is under contract with NASA. U.S. Government sponsorship acknowledged. The authors would like to thank the National Geodetic Survey for making the Kinematic Challenge data sets available to the community.

REFERENCES

Y. E. Bar-Sever, W. I. Bertiger, A. R. Dorsey, N. E. Harvey, W. Lu, K. J. Miller, M. A. Miller, L. J. Romans, A. J. Sibthorpe, J. P. Weiss, M. Garcia-Fernandez, and J. Gross. Real-time and post-processed orbit determination and positioning, U.S. Patent No. 9,057,780 B2. June 18 2015.

W. Bertiger, S. D. Desai, B. Haines, N. Harvey, A. W. Moore, S. Owen, and J. P. Weiss. Single receiver phase ambiguity resolution with gps data. *Journal of Geodesy*, 84(5):327–337, 2010.

W. Bertiger, Y. Bar-Sever, E. Bokor, M. Butala, A. Dorsey, J. Gross, N. Harvey, W. Lu, K. Miller, M. Miller, et al. First orbit determination performance assessment for the OCX navigation software in an operational environment. In *Proceedings of the 25th International Technical Meeting of The Satellite Division of the Institute of Navigation (ION GNSS+ 2012)*, 2012.

G. J. Bierman. *Factorization methods for discrete sequential estimation*. Courier Corporation, 2006.

S. Bisnath and Y. Gao. Current state of precise point positioning and future prospects and limitations. In *Observing our changing earth*, pages 615–623. Springer, 2009.

G. Blewitt. An automatic editing algorithm for gps data. *Geophysical Research Letters*, 17(3):199–202, 1990.

C. Cai, Y. Gao, L. Pan, and J. Zhu. Precise point positioning with quad-constellations: Gps, beidou, glonass and galileo. *Advances in Space Research*, 56(1):133–143, 2015.

T. M. Damiani, A. Bilich, and G. L. Mader. Evaluating Aircraft Positioning Methods for Airborne Gravimetry: First Results from GRAV-D's Kinematic GPS Processing Challenge. In *Proceedings of the 26th International Technical Meeting of The Satellite Division of the Institute of Navigation (ION GNSS+ 2013)*, 2013.

S. Desai, W. Bertiger, J. Gross, B. Haines, N. Harvey, C. Selle, A. Sibthorpe, and J. Weiss. Results from the reanalysis of global gps data in the igs08 reference frame. 2011.

J. N. Gross, Y. Gu, M. Rhudy, F. J. Barchesky, and M. R. Napolitano. On-line modeling and calibration of low-cost navigation sensors. In *AIAA Modeling and Simulation Technologies Conference*, page 6332, 2011.

P. D. Groves. *Principles of GNSS, inertial, and multisensor integrated navigation systems*. Artech House, 2013.

C. Jekeli. *Inertial navigation systems with geodetic applications*. Walter de Gruyter, 2001.

F. L. Markley and J. L. Crassidis. *Fundamentals of Spacecraft Attitude Determination and Control*, volume 33. Springer, 2014.

N. G. S. NGS. National Geodetic Survey "Kinematic GPS Challenge" `http://www.ngs.noaa.gov/GRAV-D/gpschallenge.shtml.` , 2011.

G. Petit and B. Luzum. Iers conventions (2010). Technical report, DTIC Document, 2010.

P. Rosen, S. Hensley, K. Wheeler, G. Sadowy, T. Miller, S. Shaffer, R. Muellerschoen, C. Jones, H. Zebker, S. Madsen, et al. UAVSAR: A new NASA airborne SAR system for science and technology research. In *Radar, 2006 IEEE Conference on*, pages 8–pp. IEEE, 2006.

B. L. Stevens and F. L. Lewis. *Aircraft control and simulation*. John Wiley & Sons, 2003.

C. Yigit, V. Gikas, S. Alcay, and A. Ceylan. Performance evaluation of short to long term gps, glonass and gps/glonass post-processed ppp. *Survey Review*, 46 (336):155–166, 2014.

Y. Zhang and Y. Gao. Integration of ins and un-differenced gps measurements for precise position and attitude determination. *Journal of Navigation*, 61(01):87–97, 2008.